Power Matrix of Spherical and Conical Wavestar Geometry with Linear and Circular Arrangement

Sara Jahangiri[1], Hassan Ghassemi[2], Hamid Reza Ghafari[3], Parviz Ghadimi[4]
(Received: 23 April 2022 / Revised: 28 August 2022 / Accepted: 29 August 2022)

***Abstract*— this article investigated two different arrays of Wavestar wave energy converter (WEC) with two spherical and conical WEC geometry. The boundary element method and radiation/diffraction theory have been used to evaluate the absorbed power of the Wavestar WECs under different wave heights and periods. For validation of numerical analysis, the heave position and velocity for with and without damping coefficient compare with experimental data. Single Wavestar with spherical and conical geometry under different wave periods were investigated and then two linear and circular arrays for both considering geometries compared with each other. The result shows better performance of a circular array than a linear array for all WECs. Absorbed power by the conical geometry is bigger than the spherical geometry. Besides, the maximum power is belonging to the wave period of 6s and 7s for a circular array while in a linear array the maximum power shift to wave periods of 7s and 8s.**

Keywords—**C**onical, linear and circular array, power production spherical, wave energy converter, wavestar.

I. Introduction

Wave energy converters are usually based on the installation location and divided into three groups, offshore, nearshore, and onshore. However, the power of the waves in onshore areas is lower than in the two other areas.

In terms of location near the coast, the water depth is between the deep water and shallow water area. The wave energy extraction method or the type of device operation is usually divided into five groups, including the method of overtopping wave channel, the oscillating water column (OWC) method, the roll-surge oscillation method, the heave buoy oscillation method and the attenuators method Point absorbers are small submerged buoys that absorbs wave energy through the response of heave or pitch motion to incident waves.

The buoy size is typically small compared to the dominant wavelength or the wave with the most energy at the site. In general, more than half (53%) of the developed wave energy converter designs are point absorbers, 33% are terminators, and 14% are attenuators [1].

Wavestar is one of the simplest floating-point point WECs, with only heave motion. In a Wavestar device, several buoys are in a row, and the system may have two parallel rows of floating buoys Each of these buoys is connected to a fixed platform through an arm and the platform is fixed to the seabed through several piles. The buoy's size is much smaller than the incident wavelength. In each of the buoys, the upward motion is caused by the buoyancy force caused by the waves on the buoy, while the downward motion is caused by the acceleration of gravity. During the upward motion, some of the energy is stored as potential energy, and the rest of the energy is absorbed by the power take-off (PTO) system. Whereas, in the downward motion, the potential energy stored by the buoy is released and used by the PTO system to convert more energy. Figure 1 shows two Wavestar bodies and their PTO sketch.

Passing waves through a Wavestar device, each of the semisubmersible elements in a row, rises and falls, thus generating continuous energy. As shown in Figure 2, the motion of a buoyant by a hinged arm on a fixed structure is converted into an oscillating motion to obtain the mechanical power of the system by multiplying the Wavestar angular velocity in the PTO damping coefficient. Wavestar converter array consisting of 20 spherical buoys with a diameter of 20 cm has been tested in The laboratory of Aalborg University [2]. The system's performance at the 1:40 scale of the Wavestar system was examined from 2004 to 2005. Laboratory tests were performed on a system with 40 floats of different shapes, sizes, and weights of the float at the University of Aalborg [3]. Also, from 2006 to 2011, the Wave Star I Nissum system was developed consisting of 28 vessels with a diameter of 1 m. For more than five years, the test operation of this system was carried out continuously under sea conditions [4].

Sara Jahangiri is with Department of Maritime Engineering, Amirkabir University of Technology, Tehran, Iran.
Hassan Ghassemi is with Department of Maritime Engineering, Amirkabir University of Technology, Tehran, Iran. E-mail: gasemi@aut.ac.ir
Hamid Reza Ghafari is with Department of Maritime Engineering, Amirkabir University of Technology, Tehran, Iran.
Parviz Ghadimi is with Department of Maritime Engineering, Amirkabir University of Technology, Tehran, Iran.

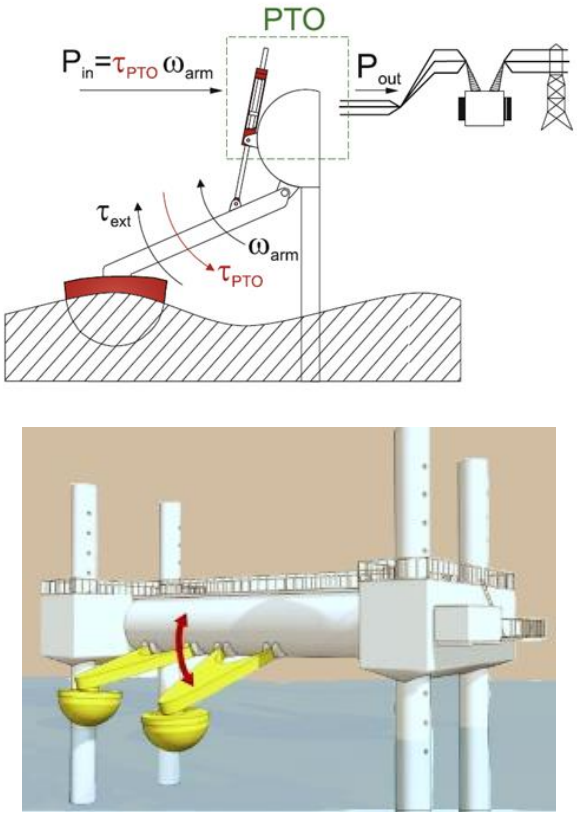

Figure. 1. Wavestar wave energy converter [5].

In 2013, the Wavestar Plymouth system was tested. The wave pool test at Plymouth University was performed on the system with a 1m diameter float, to investigate the forces acting on the bearings and the pressure on the floating shell [6,7]. In another study, from 2009 to 2013, the Wavestar Hanstholm system was developed and investigated. The evaluation of this system has been done with four years of continuous tests at sea and with the network connection. This system has two buoys with a diameter of 5m. A hydraulic power transmission system with a separate generator is used for each vessel [8-10].

In addition to experimental study, very precious work has been done related to modeling and numerical simulations to simulate Wavestar and further development and continuous improvement of the desired concepts. The boundary element method is one of the common numerical tools for floating structure analyses such as wave energy converters, floating wind turbine platforms [11], or hybrid wind-wave energy structures [12].

Hansen [13,14] investigated the enhancement of PTO power efficiently to reduce mechanical loss in the energy conversion process from the buoy to electrical energy. They applied different sea conditions to the power transmission system and numerically simulated the components of the system to study the output power of the system. Also, in several studies, physical parameters (buoy shape, the shape of array, weight, a moment of inertia) have been examined to improve system performance and increase output power. In this regard, Nambiar et al. [15] examined different strategies for controlling the Wavestar PTO system and compared them with each other. They studied the effects of PTO system control on the hydrodynamic interactions between buoys and the total power production in the range of irregular waves. The shape of the Wavestar buoy is also essential in energy production. For this purpose, Kramer et al. [16]. numerically evaluated various buoys, including disc, conical and spherical vessels. Their studies showed buoy change could improve and increase power by about 5 to 10%. Wavestar arrays have been used in hybrid wind-wave systems, including floating wind turbines and some WECs. Some researchers used Wavestar circular array with different sizes [17] and different numbers [18] mounted on a floating DeepCwind platform and Spar platform [19].

Different shapes of buoys can influence on absorbed power of WEC [20]. Different type of floater has been investigated by Ref [21] to evaluate the absorbed power by WEC. Their Resulted showed that a cone-cylinder shape floater is more suitable for WEC.

The present study deals with the comparison of spherical and conical buoy shapes for a Wavestar WEC for single and multiple Wavestar with the linear and circular array.

II. Numerical Modeling of the Hybrid System

The diffraction wave, force is obtained by calculating the pressure integral on the wetted hull body surface. This method can be used when the dimensions of the floating body are large enough compared to the wave amplitude to ignore fluid viscosity forces. Besides, the equivalent diameter of the hull, the body being large significant than wavelength to affect the wave field due to diffraction. In diffraction theory, the fluid flow field is expressed by the flow potential function. Therefore, the potential function must be valid in the Laplace equation, and also the boundary conditions such as the body surface, the free surface, and seabed boundary conditions. the infinite boundary condition known as the Summerfield condition [22] must be satisfied. Using the superposition principle of potentials, it can be stated that the total potential is combined with the three terms, including the incident wave potential, the diffraction wave potential, and the radiation potential [23]. The equation of motion in the time domain is written as follows [24].

$$\{\mathrm{m}+A_{\infty}\}\ddot{\mathrm{X}}(t)+\mathrm{c}\dot{\mathrm{X}}(t)+\mathrm{KX}(t)+\int_{0}^{t}\mathrm{R}(t-\tau)\dot{\mathrm{X}}(\tau)\,d\tau=\mathrm{F}(t) \quad (1)$$

In Equation 1, m is the structural mass matrix, $\boldsymbol{A}_{\infty}$ is the fluid added mass matrix at infinite frequency, c is the damping matrix containing the damping effects of linear radiation, K is the total stiffness matrix, and R is the velocity impact matrix. $\mathrm{F}(t)$ is total wave force, including first and second-order force. the hydrodynamic drift force can be obtained from the second-order wave force base on the BEM theory [25,26].

The acceleration impact function matrix can be used in the equation of motion, as follows:

$$h(t) = -\frac{2}{\pi}\int_0^\infty B(\omega)\frac{\sin(\omega t)}{\omega}d\omega = \frac{2}{\pi}\int_0^\infty \{A(\omega) - A_\infty\}\cos(\omega t)\,d\omega \quad (2)$$

Parameters $\mathbf{A}_{\omega}$ and $\mathbf{B}_{\omega}$ have added a mass matrix and a hydrodynamic damping matrix, respectively. Additional information on the BEM method and more detail is available in Ghafari et al [27].

III. VALIDATION

In this section, the validation of a single Wavestar has been investigated. The dimensions of the Wavestar are considered based on [28]. Figure 2 shows a schematic of a 1:5 scale model of Wavestar. The Wavestar buoy is a diameter of 527mm and connects with an arm to a pivot point that makes oscillating movement around a hinged connection by passing a wave through this floating buoy. System properties of the Wavestar for the 1:5 scale model are listed in Table1.

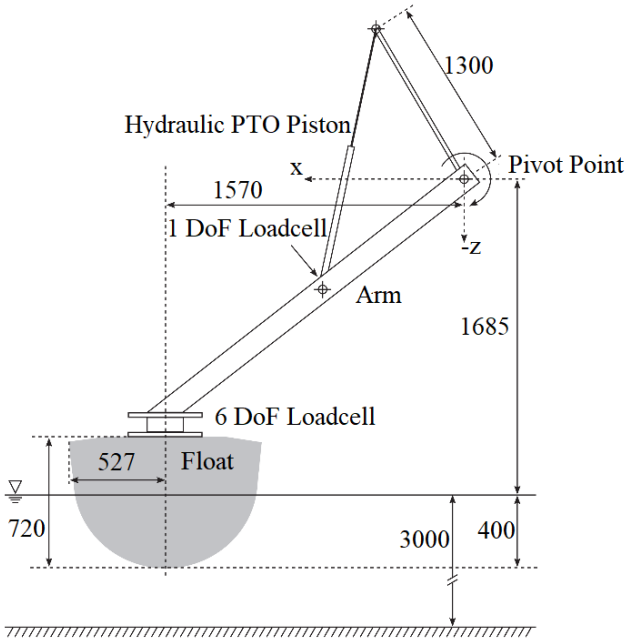

Figure. 2. The sketch of single Wavestar [28].

TABLE. 1.
SYSTEM PROPERTIES OF THE WAVESTAR FOR 1:5 SCALE MODEL.

Properties	Model	Unit
Mass (Float & Arm)	220	kg
Mass moment of Inertia	124	kg m^2
Centre of Mass (CoM) of the floating system in equilibrium relative to the hinge position:		
X	1.3954	m
Y	0.0	m
Z	-1.3305	m
Submergence (in equilibrium)	0.4	m

The experimental test used some sensors in different system locations. One sensor uses ball bearings at the pivot point with 2 force sensors considering 3 degrees of freedom (DOF). Another placed between floater and arm with 6 DOF force and torque. And one position and velocity sensor are utilized for the hydraulic piston.

Figure 3 displays the comparison of the Wavestar heave displacement and velocity between experimental and numerical results. Results are presented for damping coefficients of 0 and 200 N.m.s /(rad). It should be noted that the considered regular wave with a period of 1.4 s and wave height of 0.1 m.

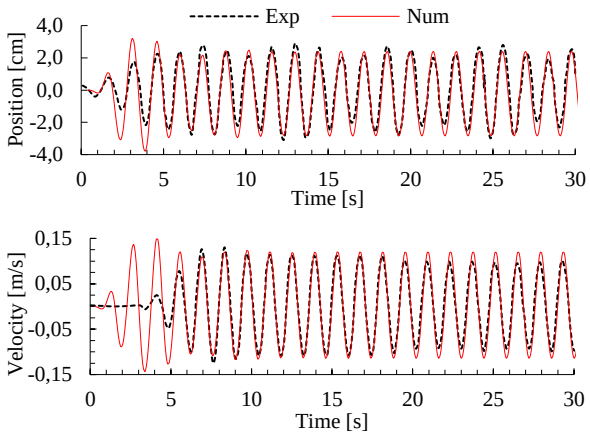

Figure. 3. Comparison of numerical and experimental time history for without damping coefficient.

As can be seen from Figure 3 the numerical result and experimental data shows the nearly equal distance between time history peak and through as well as amplitude for both Wavestar position and velocity. Furthermore, the amplitudes of position and velocity are almost the same between the numerical and experimental results.

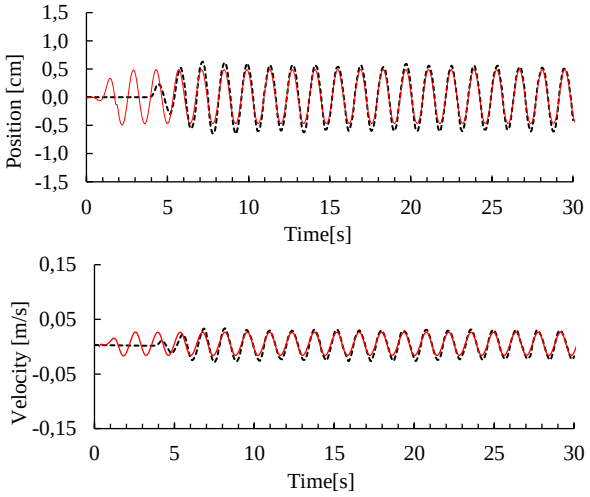

Figure. 4. Comparison of numerical and experimental time history with PTO damping coefficient ($D_{exp} = 200\ N\ m\ s$).

As shown in Figures 3 and 4, the results of the numerical solution time history provide good agreement with the experimental data. According to the validation of numerical and experimental results in the model

dimensions, another simulation is analyzed based on the prototype dimension mentioned in Table 1.

IV. RESULTS AND DISCUSSION

In this paper, the absorbed power of two Wavestar with spherical and conical geometries is compared to study the performance of this geometry with different arrangements. First, the power of the two single WECs is compared under different wave periods, then the linear array of both spherical and conical WECs as well as the circular array of these WECs is examined. Four WECs have been considered for each array.

Figure 5 shows WECs with spherical and conical geometry. It should be noted that the diameter of both WECs is 5 m based on Table 1.

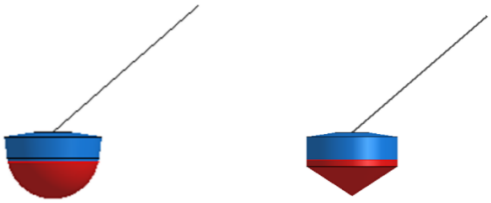

(a) spherical (b) conical

Figure. 5. Different Wavestar geometry.

Figure 6 compares the power of two selected WECs against different wave periods. The wave height is 1m, and the damping coefficient is 1.5e4 kN.m/(rad/s). As can be seen, in all incident wave periods, the absorbed power of the conical point WEC is greater than the spherical one. It can also be found that the maximum amount of WECs for both WECs belongs to the wave period of 7. In this period, the power of conical and spherical WECs is 9.6 and 8.1 kW, respectively. In general, it can be said that for a single Wavestar, the performance of conical geometry is better than spherical geometry.

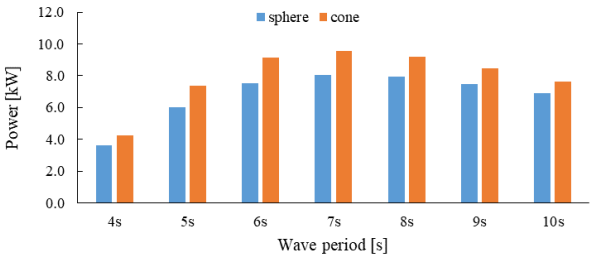

Figure. 6. Comparison of Wavestar with different geometry under different wave periods.

To better evaluate the performance of the two presented geometries, the linear arrangement of the WECs with four numbers and the incident wave angle of 0°has been studied. Figure 7 shows the linear arrangement of WECs with a distance of 10m between each adjacent WEC.

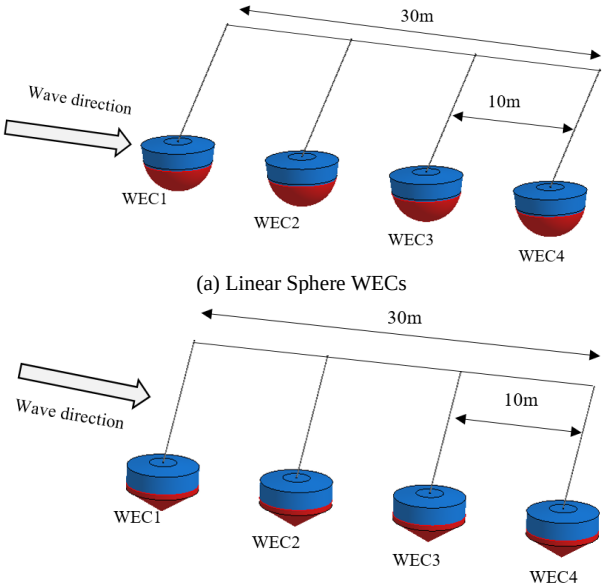

(a) Linear Sphere WECs

(b) Linear Cone WECs

Figure. 7. Linear array of WECs with different geometry.

First, the wave contour surrounding the WEC array is presented in Figure 8. As can be seen, the wave incident angle is parallel to the array direction. The incident wave height is 1m and the wave period is 4s.

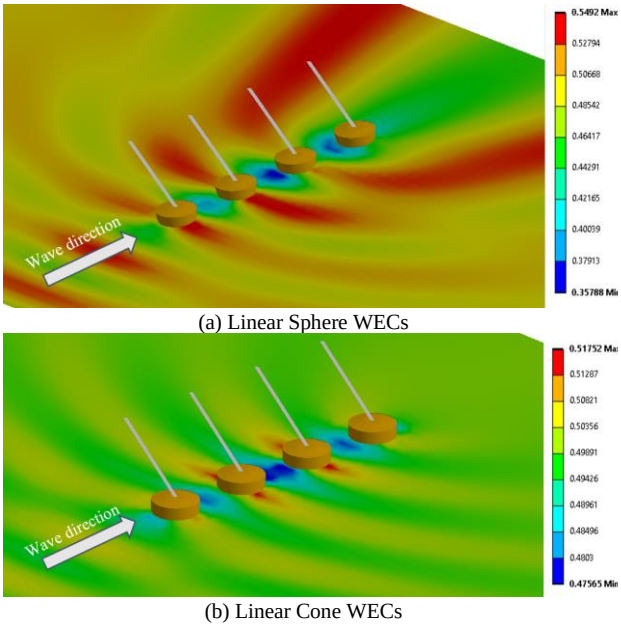

(a) Linear Sphere WECs

(b) Linear Cone WECs

Figure. 8. Wave contour around linear WECs array. T=4s H=1m.

Depending on the waves created around the WECs and the effect of each WEC on the other WECs, it is expected to different absorbed power obtained. Figure 9 presents a circular array of the two geometry WEC.

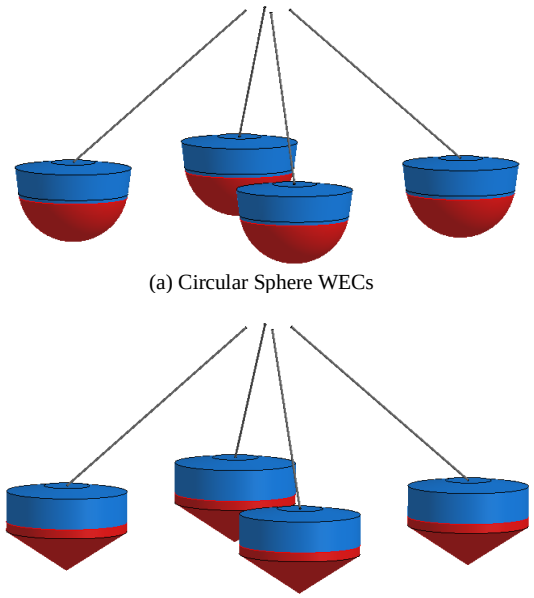

(a) Circular Sphere WECs

(b) Circular Cone WECs

Figure. 9. Circular array of WECs.

The incident wave contour around the circular array for both conical and spherical geometry is shown in Figure. 10. The angle of impact of the wave is 180 degrees. The height and period of the impact wave are 1m and 4s, respectively.

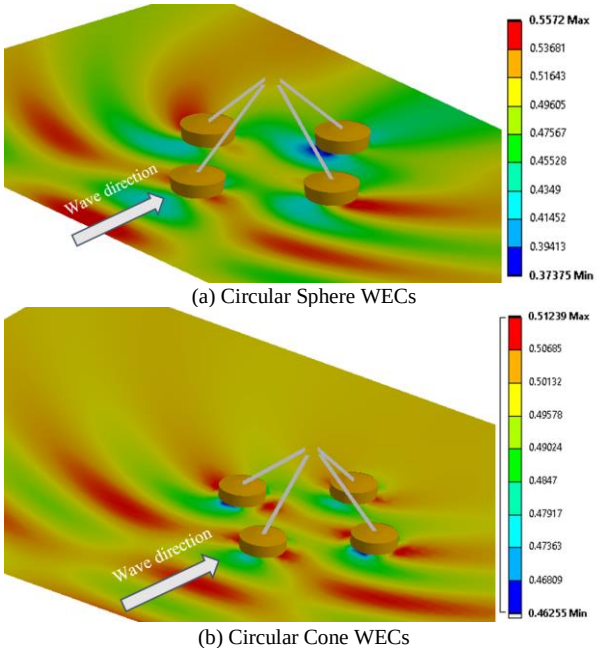

(a) Circular Sphere WECs

(b) Circular Cone WECs

Figure. 10. Wave contour around circular WECs array. T=4s H=1m.

Based on the wave contour presented in Figure 10, it can be seen that radiation and wave diffraction due to different WECs affect the wave height and wave path, and this phenomenon can change the absorbed power.

Tables 2 to 5 show the comparison of four WECs power located in a linear array for both spherical and conical case studies.

TABLE 2.
COMPARISON OF THE ABSORBED POWER MATRIX BETWEEN LINEAR AND CIRCULAR ARRAYS FOR CONICAL AND SPHERICAL GEOMETRY FOR WEC1

WEC1	H=1m	4s	5s	6s	7s	8s	9s	10s
Cone	Circular	4.1	10.0	10.6	9.7	8.8	7.9	7.2
	Linear	5.4	9.0	9.5	9.9	9.4	8.4	7.4
Sphere	Circular	4.0	8.4	8.9	8.3	7.6	7.1	6.5
	Linear	3.9	7.0	7.8	8.3	8.1	7.5	6.8
WEC1	H=2m	4s	5s	6s	7s	8s	9s	10s
Cone	Circular	12.7	30.1	32.4	32.8	32.1	30.5	28.3
	Linear	17.6	31.5	34.9	37.3	36.3	33.0	29.5
Sphere	Circular	10.4	25.1	27.3	28.0	27.9	26.9	25.3
	Linear	14.5	26.5	29.6	32.1	31.7	29.3	26.6
WEC1	H=3m	4s	5s	6s	7s	8s	9s	10s
Cone	Circular	18.3	54.7	61.3	63.9	64.6	63.2	60.2
	Linear	26.6	54.5	64.8	72.8	74.3	69.5	63.4
Sphere	Circular	19.1	51.1	56.8	59.2	59.7	58.2	55.4
	Linear	26.9	52.5	61.1	67.7	68.3	63.9	58.5
WEC1	H=4m	4s	5s	6s	7s	8s	9s	10s
Cone	Circular	-	66.8	80.8	88.8	94.5	96.6	95.7
	Linear	-	59.4	80.2	98.5	110.3	109.4	103.2
Sphere	Circular	-	67.4	80.0	88.2	93.6	95.0	93.0
	Linear	-	63.4	82.1	98.3	107.4	105.6	99.3

TABLE 3.
COMPARISON OF THE ABSORBED POWER MATRIX BETWEEN LINEAR AND CIRCULAR ARRAYS FOR CONICAL AND SPHERICAL GEOMETRY FOR WEC2

WEC2	H=1m	4s	5s	6s	7s	8s	9s	10s
Cone	Circular	4.0	8.4	8.8	8.7	8.4	7.8	7.2
	Linear	3.8	6.8	8.9	9.3	8.8	8.0	7.2
Sphere	Circular	2.9	6.6	7.1	7.3	7.2	6.9	6.4
	Linear	2.9	5.5	7.3	7.9	7.6	7.1	6.5
WEC2	H=2m	4s	5s	6s	7s	8s	9s	10s
Cone	Circular	21.3	21.1	26.6	30.6	31.7	30.7	28.5
	Linear	11.9	23.5	32.2	35.1	33.8	31.3	28.5
Sphere	Circular	21.1	19.9	23.5	26.5	27.5	27.0	25.5
	Linear	10.4	20.5	27.8	30.4	29.6	27.8	25.7
WEC2	H=3m	4s	5s	6s	7s	8s	9s	10s
Cone	Circular	43.8	39.5	48.9	58.4	62.9	63.0	60.2
	Linear	16.4	39.3	58.2	68.2	68.4	65.2	60.9
Sphere	Circular	45.4	41.6	48.6	55.5	58.5	58.0	55.4
	Linear	18.7	40.3	56.7	64.3	63.6	60.4	56.4
WEC2	H=4m	4s	5s	6s	7s	8s	9s	10s
Cone	Circular	-	57.2	65.7	81.2	91.6	95.7	95.2
	Linear	-	40.7	68.6	92.2	100.5	100.9	97.9
Sphere	Circular	-	66.2	74.6	86.8	94.0	95.3	92.8
	Linear	-	47.4	73.7	93.5	99.7	99.0	95.1

TABLE 4.
COMPARISON OF THE ABSORBED POWER MATRIX BETWEEN LINEAR AND CIRCULAR ARRAYS FOR CONICAL AND SPHERICAL GEOMETRY FOR WEC3

WEC3	H=1m	4s	5s	6s	7s	8s	9s	10s
Cone	Circular	5.6	5.7	7.3	8.2	8.3	7.9	7.2
	Linear	2.7	6.8	8.2	8.4	8.2	7.8	7.1
Sphere	Circular	5.5	5.2	6.2	6.9	7.1	6.9	6.5
	Linear	2.2	5.5	6.8	7.2	7.1	6.9	6.4
WEC3	H=2m	4s	5s	6s	7s	8s	9s	10s
Cone	Circular	12.7	30.1	32.4	32.8	32.1	30.5	28.3
	Linear	8.5	23.2	29.8	31.6	31.5	30.3	28.2
Sphere	Circular	10.4	25.1	27.3	28.0	27.9	26.9	25.4
	Linear	8.0	20.6	26.0	27.6	27.7	26.9	25.4
WEC3	H=3m	4s	5s	6s	7s	8s	9s	10s
Cone	Circular	18.3	54.7	61.3	63.9	64.6	63.2	60.2
	Linear	11.3	38.5	54.4	60.7	63.0	62.5	59.7
Sphere	Circular	19.1	51.1	56.8	59.2	59.7	58.3	55.5
	Linear	14.3	40.5	53.4	58.0	59.2	58.2	55.4
WEC3	H=4m	4s	5s	6s	7s	8s	9s	10s
Cone	Circular	-	66.8	80.7	88.8	94.5	96.6	95.7
	Linear	-	39.3	66.3	81.3	90.5	95.0	94.9

Sphere	Circular	-	67.3	80.0	88.2	93.6	95.0	93.0
	Linear	-	47.2	71.4	84.3	91.8	94.6	92.9

TABLE 5.
COMPARISON OF THE ABSORBED POWER MATRIX BETWEEN LINEAR AND CIRCULAR ARRAYS FOR CONICAL AND SPHERICAL GEOMETRY FOR WEC4

WEC4	H=1m	4s	5s	6s	7s	8s	9s	10s
Cone	Circular	4.0	8.4	8.8	8.7	8.4	7.8	7.2
	Linear	3.0	4.9	7.0	8.1	8.2	7.8	7.2
Sphere	Circular	2.9	6.6	7.1	7.3	7.2	6.9	6.4
	Linear	2.6	4.1	5.8	6.8	7.1	6.9	6.5
WEC4	H=2m	4s	5s	6s	7s	8s	9s	10s
Cone	Circular	12.8	34.4	38.5	36.5	33.7	31.1	28.5
	Linear	9.7	16.4	24.7	29.9	31.4	30.6	28.5
Sphere	Circular	15.1	31.7	33.9	32.0	29.8	27.7	25.7
	Linear	9.5	15.1	21.9	26.1	27.5	27.1	25.6
WEC4	H=3m	4s	5s	6s	7s	8s	9s	10s
Cone	Circular	16.9	53.8	68.4	70.7	68.4	64.9	60.9
	Linear	14.8	26.1	42.8	55.7	62.0	62.9	60.4
Sphere	Circular	26.9	55.8	64.9	65.8	63.6	60.3	56.6
	Linear	18.1	29.4	44.1	54.3	58.6	58.7	56.0
WEC4	H=4m	4s	5s	6s	7s	8s	9s	10s
Cone	Circular	-	56.5	75.7	85.1	90.3	93.1	93.9
	Linear	-	25.3	47.4	70.1	86.3	94.6	95.7
Sphere	Circular	-	66.0	76.5	82.3	86.2	88.9	89.5
	Linear	-	33.3	55.6	75.8	88.9	94.5	93.7

As can be seen from Tables 2 to 5, in all incident wave periods, the absorbed power by the conical geometry is bigger than the spherical geometry. Besides comparison of different arrangements shows better performance of a circular array than a linear array for all WECs under different wave heights and wave periods. As can be seen in all wave heights, the maximum power is belonging to the wave period of 6s and 7s for a circular array while in a linear array the maximum power shift to wave periods of 7s and 8s. In addition, it can be found that wave periods of 4s give lower absorbed power by all WECs in all arrangements and geometry.

WECs 2 and 4 have the same power due to symmetry than the incident wave direction, while significant differences can be seen for that of WECs 1 and 3. In greater wave periods, the power difference between the different WECs is negligible, which means that the effects of radiation and diffraction waves are the same on all four WECs. Finally, it should be noted that, in general, the harvesting power of WECs with conical geometry is more than spherical WECs.

By increasing the wave period, the difference between the absorbed power between WEC1 to WEC4 is negligible, while in shorter wave periods, a significant difference is observed. It can also be found that the power of upstream WECs (i.e. WEC1) is higher than that of downstream WECs (i.e. WEC4). Table 6 compares the total absorbed power matrix between linear and circular arrays for conical and spherical geometry.

TABLE 6.
COMPARISON OF THE TOTAL ABSORBED POWER MATRIX BETWEEN LINEAR AND CIRCULAR ARRAYS FOR CONICAL AND SPHERICAL GEOMETRY.

Total	H=1m	4s	5s	6s	7s	8s	9s	10s
Cone	Circular	18	33	35	35	34	31	29
	Linear	15	27	34	36	35	32	29
Sphere	Circular	15	27	29	30	29	28	26
	Linear	12	22	28	30	30	28	26
Total	H=2m	4s	5s	6s	7s	8s	9s	10s
Cone	Circular	59	116	130	133	130	123	114
	Linear	48	95	122	134	133	125	115
Sphere	Circular	57	102	112	115	113	108	102
	Linear	42	83	105	116	117	111	103
Total	H=3m	4s	5s	6s	7s	8s	9s	10s
Cone	Circular	97	203	240	257	260	254	241
	Linear	69	158	220	257	268	260	244
Sphere	Circular	111	200	227	240	241	235	223
	Linear	78	163	215	244	250	241	226
Total	H=4m	4s	5s	6s	7s	8s	9s	10s
Cone	Circular	-	247	303	344	371	382	381
	Linear	-	165	263	342	388	400	392
Sphere	Circular	-	267	311	346	367	374	368
	Linear	-	191	283	352	388	394	381

As can be seen from Table 6 increasing wave height from 1 m to 2 m, 3 m, and 4 m leads to an average power increase of 3.8, 7.6, and 12 times, respectively. Also in all wave heights, the maximum power is belonging to the wave period of 7s for both circular array and linear array.

V. CONCLUSION

In this paper, the effect of geometry on the absorbed power of a Wavestar WEC is compared. Two spherical and conical geometries are considered as WEC buoys. The meshing method of the present work is based on the BEM theory, and the method of simulating a floating body in a wave is based on the three-dimensional diffraction/radiation theory. First, in order to perform the validation, the power of numerical results is compared with the experimental data of a spherical WEC for with and without PTO damping coefficient. Then the linear and circular array of the WECs were investigated to compare the absorbed power of both geometries. The results showed that for a single WEC, the conical geometry has a higher power than the spherical geometry and the maximum power is obtained in a wave period of 7s. Also, the comparison between linear and circular arrays shows that with increasing incident wave period, the difference between the absorbed powers decreases, while in shorter wave periods, there is a significant difference. The result shows better performance of circular array than linear array for all WECs. Absorbed power by the conical geometry is bigger than the spherical geometry. Besides, the maximum power is belonging to the wave period of 6s and 7s for a circular array while in linear array the maximum power shift to wave periods of 7s and 8s.

REFERENCES

[1] IRENA, 2014. Wave Energy. Technology Brief. 2014, IRENA Abu Dhabi, UAE.

[2] Kofoed JP. Indledende hydrauliske undersøgelser af bølgeenergianlægget Bartholins roterende. 2001.

[3] Frigaard PB, Andersen TL, Kofoed JP, Kramer MM, Ambühl S. Wavestar Energy Production Outlook. 2016.

[4] Frigaard P, Lyke Anderson T. Effektmalinger pa Wave Star i nissum bredning. Tech. Rep. 61, Aalborg University, Denmark; 2008.

[5] Pedersen HC, Hansen RH, Hansen AH, Andersen TO, Bech MM. Design of full scale wave simulator for testing Power Take Off

systems for wave energy converters. International Journal of Marine Energy. 2016 Apr 1; 13:130-56.

[6] Jakobsen M. Technical report on wave-structure interactions on point absorbe. tech. rep., Aalborg University; 2014.

[7] Jakobsen MM, Beatty S, Iglesias G, Kramer MM. Characterization of loads on a hemispherical point absorber wave energy converter. International Journal of Marine Energy. 2016 Apr 1; 13:1-5.

[8] Kramer M, Marquis L, Frigaard P. Performance evaluation of the wavestar prototype. In9th ewtec 2011: Proceedings of the 9th European Wave and Tidal Conference, Southampton, UK, 5th-9th September 2011 2011. University of Southampton.

[9] Vidal ES, Hansen RH, Kramer M. Early performance assessment of the electrical output of Wavestar's prototype. InProceedings of the 4th International Conference on Ocean Energy, 17 October, Dublin 2012 Oct 17.

[10] Marquis L. Wavestar-4 years of continuous operation in the North Sea. InInternational Conference on Ocean Energy ICOE 2014.

[11] Neisi A, Ghassemi H, Iranmanesh M, He G. Effect of the multi-segment mooring system by buoy and clump weights on the dynamic motions of the floating platform. Ocean Engineering. 2022 Sep 15; 260:111990.

[12] Ganjgani AA, Ghafari HR, Ghassemi H, Ghiasi M. Investigation of Buoy Size and Location on Hydrodynamic Response and Mooring Tension of the DeepCwind Floating Wind Turbine. American Journal of Civil Engineering and Architecture. 2022;10(1):1-7.

[13] Hansen RH. Design and control of the powertake-off system for a wave energy converter with multiple absorbers. Department of Energy Technology, Aalborg University; 2013.

[14] Hansen AH. Investigation and optimisation of a discrete fluid power PTO-system for wave energy converters. Department of Energy Technology, Aalborg University; 2014 Jun.

[15] Nambiar AJ, Forehand DI, Kramer MM, Hansen RH, Ingram DM. Effects of hydrodynamic interactions and control within a point absorber array on electrical output. International Journal of Marine Energy. 2015 Apr 1; 9:20-40.

[16] Kramer M, Brorsen M, Frigaard P. Wave Star: Indledende undersøgelse af flydergeometri. 2004.

[17] Ghafari HR, Ghassemi H, Neisi A. Power matrix and dynamic response of the hybrid Wavestar-DeepCwind platform under different diameters and regular wave conditions. Ocean Engineering. 2022 Mar 1; 247:110734.

[18] Ghafari HR, Neisi A, Ghassemi H, Iranmanesh M. Power production of the hybrid Wavestar point absorber mounted around the Hywind spar platform and its dynamic response. Journal of Renewable and Sustainable Energy. 2021 May 15;13(3):033308.

[19] Ghafari HR, Ghassemi H, He G. Numerical study of the Wavestar wave energy converter with multi-point-absorber around DeepCwind semisubmersible floating platform. Ocean Engineering. 2021 Jul 15; 232:109177.

[20] Homayoun E, Ghassemi H, Ghafari H. Power performance of the combined monopile wind turbine and floating buoy with heave-type wave energy converter. Polish Maritime Research. 2019.

[21] Gaspar J, Kamarlouei M, Calvário M, Soares CG. FOWT with Controllable Waterplane Area. In2017 INORE North American Symposium, May 19–22, Portland, Oregon 2017.

[22] Dhanak MR, Xiros NI, editors. Springer handbook of ocean engineering. Springer; 2016 Jul 23.

[23] Ghafari H, Dardel M. Parametric study of catenary mooring system on the dynamic response of the semi-submersible platform. Ocean Engineering. 2018 Apr 1; 153:319-32.

[24] Cummins WE, Iiuhl W, Uinm A. The impulse response function and ship motions.1962.

[25] Motallebi M, Ghafari H, Ghassemi H, Shokouhian M. Calculating the second-order hydrodynamic force on fixed and floating tandem cylinders. Zeszyty Naukowe Akademii Morskiej w Szczecinie. 2020.

[26] Ghafari H, Motallebi M, Ghassemi H. Potential-based boundary element method to calculate the hydrodynamic drift force on the floating cylinder. Journal of Applied Mathematics and Computational Mechanics. 2020;19(4).

[27] Ghafari HR, Ketabdari MJ, Ghassemi H, Homayoun E. Numerical study on the hydrodynamic interaction between two floating platforms in Caspian Sea environmental conditions. Ocean Engineering. 2019 Sep 15; 188:106273.

[28] Windt C, Davidson J, Ransley EJ, Greaves D, Jakobsen M, Kramer M, Ringwood JV. Validation of a CFD-based numerical wave tank model for the power production assessment of the wavestar ocean wave energy converter. Renewable Energy. 2020 Feb 1; 146:2499-516.